In vivo PET Imaging of [^{11}C]CIMBI-5, a 5-HT$_{2A}$R Agonist Radiotracer in Nonhuman Primates

Jaya Prabhakaran[1,2], Christine DeLorenzo[3], Francesca Zanderigo[1,2], Gitte M. Knudsen[4], Nic Gillings[5], Mali Pratap[2], Matthew J. Jorgensen[6], James Daunais[7], Jay R. Kaplan[6], Ramin V. Parsey[3], J. John Mann[1,2], and J.S. Dileep Kumar[2*]

[1]Department of Psychiatry, Columbia University Medical Center, New York, USA. [2]Area of Molecular Imaging and Neuropathology, New York State Psychiatric Institute, New York, USA. [3]Department of Psychiatry, Stony Brook University School of Medicine, Stony Brook, New York, USA. [4]Neurobiology Research Unit and Center for Integrated Molecular Brain Imaging, Rigshospitalet and University of Copenhagen, Denmark. [5]Department of Clinical Physiology, Nuclear Medicine and PET, Copenhagen University Hospital Rigshospitalet, Denmark. [6]Department of Pathology, Section on Comparative Medicine, Wake Forest School of Medicine, Winston-Salem, North Carolina, USA. [7]Department of Physiology and Pharmacology, Wake Forest University Medical Center Winston-Salem, North Carolina, USA.

Received, December 24, 2018; Accepted, July 9, 2019; Published, July 20, 2019.

ABSTRACT - Purpose: 5-HT$_{2A}$R exists in high and low affinity states. Agonist PET tracers measure binding to the active high affinity site and thus provide a functionally relevant measure of the receptor. Limited *in vivo* data have been reported so far for a comparison of agonist versus antagonist tracers for 5-HT$_{2A}$R used as a proof of principle for measurement of high and low affinity states of this receptor. We compared the *in vivo* binding of [^{11}C]CIMBI-5, a 5-HT$_{2A}$R agonist, and of the antagonist [^{11}C]M100907, in monkeys and baboons. **Methods:** [^{11}C]CIMBI-5 and [^{11}C]M100907 baseline PET scans were performed in anesthetized male baboons (n=2) and male vervet monkeys (n=2) with an ECAT EXACT HR+ and GE 64-slice PET/CT Discovery VCT scanners. Blocking studies were performed in vervet monkeys by pretreatment with MDL100907 (0.5 mg/kg, i.v.) 60 minutes prior to the scan. Regional distribution volumes and binding potentials were calculated for each ROI using the likelihood estimation in graphical analysis and Logan plot, with either plasma input function or reference region as input, and simplified reference tissue model approaches. **Results:** PET imaging of [^{11}C]CIMBI-5 in baboons and monkeys showed the highest binding in 5-HT$_{2A}$R-rich cortical regions, while the lowest binding was observed in cerebellum, consistent with the expected distribution of 5-HT$_{2A}$R. Very low free fractions and rapid metabolism were observed for [^{11}C]CIMBI-5 in baboon plasma. Binding potential values for [^{11}C]CIMBI-5 were 25-33% lower than those for [^{11}C]MDL100907 in the considered brain regions. **Conclusion:** The lower binding potential of [^{11}C]CIMBI-5 in comparison to [^{11}C]MDL100907 is likely due to the preferential binding of the former to the high affinity site *in vivo* in contrast to the antagonist, [^{11}C]MDL100907, which binds to both high and low affinity sites.

INTRODUCTION

The serotonin 2A receptor (5-HT$_{2A}$R) is the most abundant excitatory serotonin (5-HT) receptor in the human brain and it plays an essential role in a number of physiological processes and psychiatric disorders, including schizophrenia, major depression, suicidal behavior, aggression, neurodegenerative disorders, addiction and pain (1-4). Drugs with 5-HT$_{2A}$R antagonism are widely used in psychiatric disorders and hallucinogenic 5-HT$_{2A}$R agonists have been examined for treatment of depression, alcoholism, drug addiction, and pain (5-8). In the central nervous system (CNS), 5-HT$_{2A}$R are abundant in cortical and forebrain areas, whereas comparatively lower density is found in hippocampus; the least expression has been detected in striatum and cerebellum (9-16). Positron emission tomography (PET) imaging enables quantification of 5-HT$_{2A}$R and measurement of receptor occupancy by therapeutic drug candidates *in vivo* (17-18). [^{11}C]MDL100907 ([^{11}C]M100907 *aka* [^{11}C]volinanserin) and [^{18}F]altanserin have been so far the most commonly used antagonist ligands for *in vivo* PET studies of 5-HT$_{2A}$R (17-19). Antagonist ligands bind to the high affinity (HA) and low affinity (LA) conformations of 5-HT$_{2A}$R with equal affinity (10). In contrast, agonists ligands at tracer doses, as used in PET, bind preferentially to the HA

Corresponding Author: J. S. Dileep Kumar, PhD. Area of Molecular Imaging and Neuropathology**,** New York State Psychiatric Institute, 1051 Riverside Drive**,** New York, NY 10032**;** Email: kumardi@nyspi.columbia.edu

state of the receptor with high affinity, which is coupled to G-protein and thereby provides a more meaningful functional measure of the 5-HT_{2A}R (10, 20-23). Sequential PET scans performed with both an agonist and antagonist 5-HT_{2A}R tracer in the same subject may enable the quantification of binding to active or G-protein-coupled receptors (GPCR) and help estimate the ratio of coupled to uncoupled receptors (21,22). This ratio reflects the capacity of the receptor for signal transduction. The classical approach to determine relative levels of high and low affinity 5-HT_{2A}Rs is by measuring the binding maximum (B_{max}) and dissociation constant (K_D) using a two-site model (21,22). This can be achieved *in vitro* by administering the agonist radiotracer in a sufficient concentration range to determine the B_{max} for both sites. However, this approach may not be feasible *in vivo* since it would require injection of high pharmacological doses of the radioligand, which may be prohibited in humans. As an alternative approach, we set out to determine the HA and total 5-HT_{2A}R binding *in vivo* by comparing agonist and antagonist radiotracer bindings using PET imaging.

There are several efforts reported with limited success, towards the development of agonist radiotracers for 5-HT_{2A}R. Among these, [^{11}C]CIMBI-5 ([^{11}C]IDME or [^{11}C]25I-NBMeO) (Figure 1) was the first successful 5-HT_{2A}R agonist tracer evaluated in pigs and non-human primates *in vivo* (24-27). CIMBI-5 belongs to the *N*-benzylphenethylamine class of 5-HT_{2A}R agonists and exhibits high affinity to 5-HT_{2A}R (K_i = 0.15 nM, E_{max} = 81%, EC_{50} = 0.44 nM) (24-27). Competitive binding assay from the Psychoactive Drug Screening Program (PDSP) of the National Institute of Mental Health (NIMH) shows that CIMBI-5 has equivalent affinity to 5-HT_{2B}R and a threefold higher affinity to 5-HT_{2C}R than to 5-HT_{2A}R and did not have significant affinity for various other brain targets (24). Recently, [^{11}C]CIMBI-36 (K_i = 0.5 nM, E_{max} = 87%), the bromo-analogue of CIMBI-5, has been reported to have comparable specific to non-specific binding ratio as of [^{11}C]CIMBI-5 in pig and non-human primates; including receptor occupancy in pig brain and fenfluramine induced endogenous changes in monkeys (28-31). Subsequently, [^{11}C]CIMBI-36 has been studied in human and thus it is so far the only 5-HT_{2A}R agonist PET tracer studied in human (32). Although the time activity curves (TACs) of [^{11}C]CIMBI-36 showed better cortex to cerebellum binding in nonhuman primates, the tracer suffers a slow washout in high 5-HT_2R density cortical regions and modest target to non target ratios ($\leq$1.5) in human. However, [^{11}C]CIMBI-36 exhibits excellent test-retest reproducibility in human subjects and shows a high correlation with antagonist PET ligand [^{18}F]altanserin (33). Also, hippocampus and choroid plexus regions show higher binding with [^{11}C]CIMBI-36 than [^{18}F]altanserin. This may be due to off target binding of [^{11}C]CIMBI-36 to 5-HT_{2C}Rs (33). Also, hippocampus and choroid plexus regions show higher binding with [^{11}C]CIMBI-36 than [^{18}F]altanserin. This may be due to off target binding of [^{11}C]CIMBI-36 to 5-HT_{2C}Rs (33). More recently, several fluoro-analogues of CIMBI-36 were reported, including [^{18}F]FECIMBI-36, with limited success *in vivo* (34-37). [^{11}C]CIMBI-5 is the first generation high affinity 5-HT_{2A}R agonist PET tracer, which possesses comparable affinity to the recently reported [^{11}C]CIMB-36 but a slightly better selectivity to 5-HT_{2A}R (28). Therefore we believed it is a meaningful idea to test [^{11}C]CIMBI-5 and performed the evaluation of [^{11}C]CIMBI-5 in non-human primate species. Herein, we report the *in vivo* brain distribution of the most potent 5-HT_{2A}R agonist, [^{11}C]CIMBI-5, assessed with PET in monkeys and baboons, along with a comparison of these results with the 5-HT_{2A}R antagonist radiotracer [^{11}C]MDL100907 distribution in baboon brain.

MATERIALS AND METHODS

Materials

The commercial chemicals and solvents used in the synthesis were purchased from Sigma-Aldrich Chemical Co. (St. Louis, MO), Fisher Scientific Inc. (Springfield, NJ), or Lancaster (Windham, NH) and were used without further purification. MDL100907 and desmethyl-MDL100907 were purchased from ABX Advanced Biochemical Compounds. Analytical grade reagents were purchased from standard commercial sources. HPLC analyses were performed using a Waters 1525 binary HPLC system. The parent fractions and metabolites were collected from HPLC system coupled with γ-detector and measured using Packard Instruments Gamma Counter (Model E5005, Downers Grove, IL). [^{11}C]CO_2 was produced from RDS112 cyclotron (Siemens, Knoxville, TN) or PET Trace GE cyclotron. For detection of radiolabeled products, gamma ray detector (Bioscan Flow-Count fitted with a NaI detector) was used in series with the UV detector (Waters Model 996 set at 254 nm). Data

acquisition for both the analytical and preparative systems was accomplished using a Waters Empower Chromatography System. The specific activities were determined at the end of synthesis (EOS) based on the UV absorption and concentration standard curves (λ = 254 nm). PET imaging were performed in baboon using an ECAT EXACT HR+ scanner (Siemens, Knoxville, TN). All animal experiments were carried out with the approval of the Institutional Animal Care and Use Committee (IACUC) of Columbia University Medical Center, New York State Psychiatric Institute and Wake Forest University Medical Center.

Chemistry and Radiochemistry

CIMBI-5 and the corresponding radiolabeling precursor were synthesized by reported procedures (24-27). The radiosyntheses of [^{11}C]CIMBI-5 and [^{11}C]MDL100907 were performed by minor modifications of published methods [24-27]. Briefly, [^{11}C]CIMBI-5 was synthesized by transfer of [^{11}C]MeOTf, to a vial containing ~0.5 mg of desmethyl-N-boc protected precursor in 400 μL of acetonitrile containing 5 μL of 2M NaOH at room temperature. To the resulting solution, 250 μL of trifluoroacetic acid: acetonitrile (1:1) was added and the mixture was heated at 80 ºC for 4 min. After neutralization with 750 μL of 2M NaOH, the reaction mixture was purified through a semi HPLC (Phenomenex Prodigy™ ODS-prep, 250 x 10 mm, 10 μ; 35% acetonitrile: 65 % 0.1 M ammonium formate solution in water containing 0.5% acetic acid, 10 mL/min). The product fraction based on γ-detector was collected, diluted with 100 mL water and passed through a C-18 Sep-Pak cartridge, washed with 5 mL of 12.5 mM NaOH solution, 10 mL of water and eluted with 1 mL of ethanol. A portion of radioproduct was used for quality control studies using analytical HPLC for purity and specific activity measurements (Phenomenex Prodigy™ ODS3 250 x 4.6 mm, 5 μ; 40% acetonitrile: 60% 0.1 M ammonium formate solution in water containing 0.5% acetic acid; 2 mL/min, wavelength: 254 nm). The remaining ethanol solution was diluted with 9 mL of normal saline and filtered through a 0.22 μm sterile filter into a sterile vial for further studies.

[^{11}C]MDL100907 was synthesized by trapping [^{11}C]MeOTf into a solution of desmethyl-MDL100907 (~ 0.5 mg) in acetone (400 μL) containing 5 μL of 2N NaOH at room temperature. At the end of the trapping, the reaction mixture was directly injected into a semi preparative HPLC column (Phenomenex Prodigy™ ODS-prep, 250 x 10 mm, 10 μ, 25% acetonitrile: 75% 0.1 N ammonium acetate in water and 0.5% acetic acid; 10 mL/min). The product fraction based on γ-detector was collected, diluted with 100 mL deionized water and passed through a classic C-18 Sep-Pak cartridge. The Sep-Pak was washed with 10 mL of deionized water and the product was then eluted with 1 mL of ethanol. A small portion of the ethanol solution was analyzed by analytical HPLC (Phenomenex Prodigy™ ODS-3, 250 x 4.6 mm, 5 μ, 30% acetonitrile: 70% 0.1 N ammonium acetate in water containing 0.5% acetic acid; 2 mL/min, wavelength: 254 nm) to determine the molar activity and radiochemical purity. The remaining ethanol solution was diluted with 9 mL of normal saline and filtered through a 0.22 μm sterile filter into a sterile vial.

PET Imaging studies in monkeys and baboons

Magnetic resonance imaging (MRI) brain scans were acquired for each animal on a GE 1.5-T Signa Advantage system. Regions of interests (ROIs) were drawn on the MRI using MEDX software (Sensor Systems, Inc., Sterling, VA). PET scans were performed in two male baboons and two male vervet monkeys with an ECAT EXACT HR+ scanner (CPS/Knoxville, TN) and GE 64-slice PET/CT Discovery VCT Scanner (General Electric Medical Systems, Milwaukee, WI, USA), respectively. The fasted animals were anesthesia-inducted with ketamine (10 mg/kg i.m.) and subsequently anesthetized with 1.5–2.0% isoflurane via an endotracheal tube. Core temperature was kept constant at 37°C with a heated water blanket. An intravenous infusion line with 0.9% NaCl was maintained during the experiment and used for hydration and radiotracer injection. In the case of the baboons, an arterial line was placed to collect arterial blood samples for determination of a metabolite-corrected input function. The head was positioned at the center of the field of view, and a 10 min transmission scan was performed before the tracer injection. For each scan, [^{11}C]CIMBI-5 (185 ± 18 MBq, molar activity of 74 ± 18 GBq/μmol, n=6) or [^{11}C]M100,907 (148 ± 18 MBq, specific activity of 111 ± 18 GBq/ μmol, n=2) were injected as an i.v. bolus and PET data were collected for 120 min in 3-D mode. In the baboons, arterial blood samples were taken every 10 s for the first 2 min, using an automatic system, and manually thereafter for a total of 27 samples over 120 minutes. Blocking studies

were performed in vervet monkeys by pretreatment with MDL100907 (0.5 mg/kg i.v.) 60 minutes prior to the PET scan. PET images were each co-registered with the MRI using FLIRT. ROIs drawn on the animal's MRI scan were transferred to co-registered automated image registration (AIR) frames of PET data. Time activity curves (TACs) in the right and left regions were averaged into one TAC per region.

Protein binding and metabolite analyses

The methods for protein binding of [^{11}C]MDL100907 and [^{11}C]CIMBI-5 in baboon blood samples used in the experiments reported here are described elsewhere [25-27, 38]. The percentages of unchanged radiotracers radioactivity in plasma were determined by HPLC (25-27, 39). Blood samples (2 mL per time point) taken at 2, 12, 30, 60, and 90 min after radioactivity injection were considered for metabolites analyses. Briefly, the supernatant liquid obtained after centrifugation of the blood sample at 3,400 rpm for 10 min was transferred (0.5 mL) into a tube and mixed with acetonitrile (0.7 mL). The resulting mixture was vortexed for 10 s, and centrifuged at 14,000 rpm for 4 min. The supernatant liquid (~1 mL) was removed, the radioactivity was measured in a well-counter, and the majority (~0.8 mL) was subsequently injected onto the HPLC column (Phenomenex Prodigy™ 5 µm ODS-3, 250 x 4.6 mm; mobile phase: acetonitrile/ 25 mM Na_2HPO_4 in water, 40:60 (v/v), flow rate: 2 ml/min, retention time: 7 min) equipped with a series of radioactivity detectors. The metabolite and parent fractions collected from HPLC were analyzed using a Bioscan gamma detector. All the acquired data were then subjected to correction for background radioactivity and physical decay to calculate the percentage of the parent compound in the plasma at different time points.

Image Analysis

PET data were reconstructed with attenuation correction using the transmission data, and scatter correction was performed using model-based scatter correction (40). The reconstruction filter and estimated image filter were Shepp 0.5, the axial (Z) filter was all pass 0.4, and the zoom factor was 4.0. Final image resolution at center of field of view was 5.1 mm FWHM (41, 42). For experiments where arterial blood samples were available, distribution volumes (V_T), and corresponding binding potentials BP_P and BP_{ND}, were calculated for each ROI using the likelihood estimation in graphical analysis (LEGA), and the Logan plot; for experiments without arterial blood samples, LEGA and Logan plot with a reference region as input, and simplified reference tissue model (SRTM), were used to calculate the binding potential BP_{ND} (43, 44). Cerebellum was used as the reference region for both tracers. For experiments where arterial blood samples were available, brain TACs were corrected for vascular contribution by assuming a 5% blood volume (V_B) in the ROIs before applying LEGA or Logan plot (44). V_T (ml of plasma/ml of tissue) is defined as the ratio of the tracer concentration in the ROI to the metabolite-corrected plasma concentration of the tracer at equilibrium and represents the sum of the specific and non-displaceable distribution volumes (V_{ND}). BP_P refers to the ratio at equilibrium of specifically bound radioligand to that of total parent radioligand in plasma (i.e., free plus protein bound). BP_P in each ROI was obtained from the V_T values as $BP_P = V_T - V_{ND}$, with V_{ND} estimated using the distribution volume in the cerebellum. BP_P relates to B_{avail} as $f_P * B_{avail}/K_D$, where f_P is the plasma free fraction, B_{avail} is the density of 5-HT_{2A}R available to bind to the radiotracer, and K_D the affinity for the target of the radioligand in question. BP_{ND} (= BP_P/V_{ND}) refers to the ratio at equilibrium of specifically bound radioligand to that of non-displaceable radioligand in tissue and compares the concentration of radioligand in receptor-rich to receptor-free regions (50).

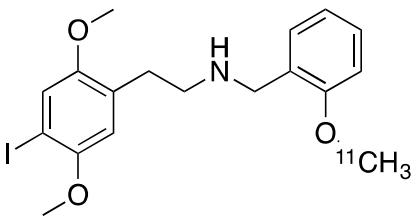

[^{11}C]CIMBI-5

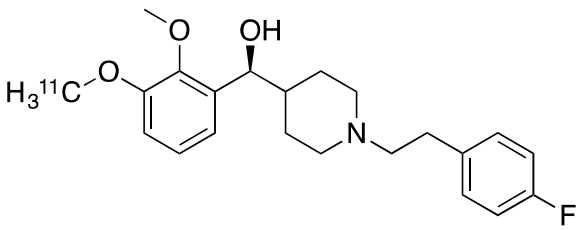

[^{11}C]MDL100907

Figure 1. Chemical structures of [^{11}C]CIMBI-5 and [^{11}C]MDL100907

RESULTS

Chemistry and Radiochemistry

The nonradioactive standard CIMBI-5 and its precursor for radiolabeling were synthesized from 2-(4-iodo-2,5-dimethoxyphenyl)ethan-1-amine in 2 steps with an overall yield of 65%. Radiolabeling was then achieved in 2 steps in a one-pot reaction with 30% yield (EOS) and a molar activity in the range of 100±37 GBq/μmole. [^{11}C]MDL100907 was, however, synthesized in 20% yield (EOS) with a molar activity 120±37 GBq/μmole (Figure 1).

PET studies of [^{11}C]CIMBI-5 in monkey

PET imaging experiments in anesthetized vervet monkeys show that [^{11}C]CIMBI-5 penetrates the blood brain barrier (BBB) and accumulates in brain (Figure 2). Specific binding of [^{11}C]CIMBI-5 to 5-HT$_{2A}$R was determined by performing blocking studies with MDL100907. The TACs for [^{11}C]CIMBI-5 in a representative monkey brain are reported in Figure 3 for both baseline and blocking scan.

Cortical regions exhibited the most uptake of the radiotracer, whereas, hippocampus showed moderate binding; caudate, putamen and cerebellum showed low uptake of [^{11}C]CIMBI-5. Slow washout of radioactivity was found in cortical regions, whereas, the TACs showed that the clearance of radiotracer was relatively faster from caudate, putamen and cerebellum. Cortex to cerebellum ratio was in the ranges of 1.7 to 1.4 at 120 minutes post injection, with and highest binding ratios were found in anterior cingulate (ACN) and medial prefrontal cortex (MED) (1.7). Hippocampus has moderate binding (HIP: CER = 1.3), whereas, putamen (1.15) and caudate (1.04) showed least binding ratios to cerebellum. Blocking studies with 5-HT$_{2A}$R antagonist MDL100907 indicate a displacement of radioactivity across the brain regions (Figure 3) where 5-HT$_{2A}$R is present. Cortical regions show moderate displacement of [^{11}C]CIMBI-5 activity (~30-50%), hippocampus (25%), caudate (-5%), putamen (3.3%) and cerebellum (12%) after pretreatment with MDL100907. Hence, caudate, putamen and cerebellum showed the least displacement of radioactivity during blocking experiments.

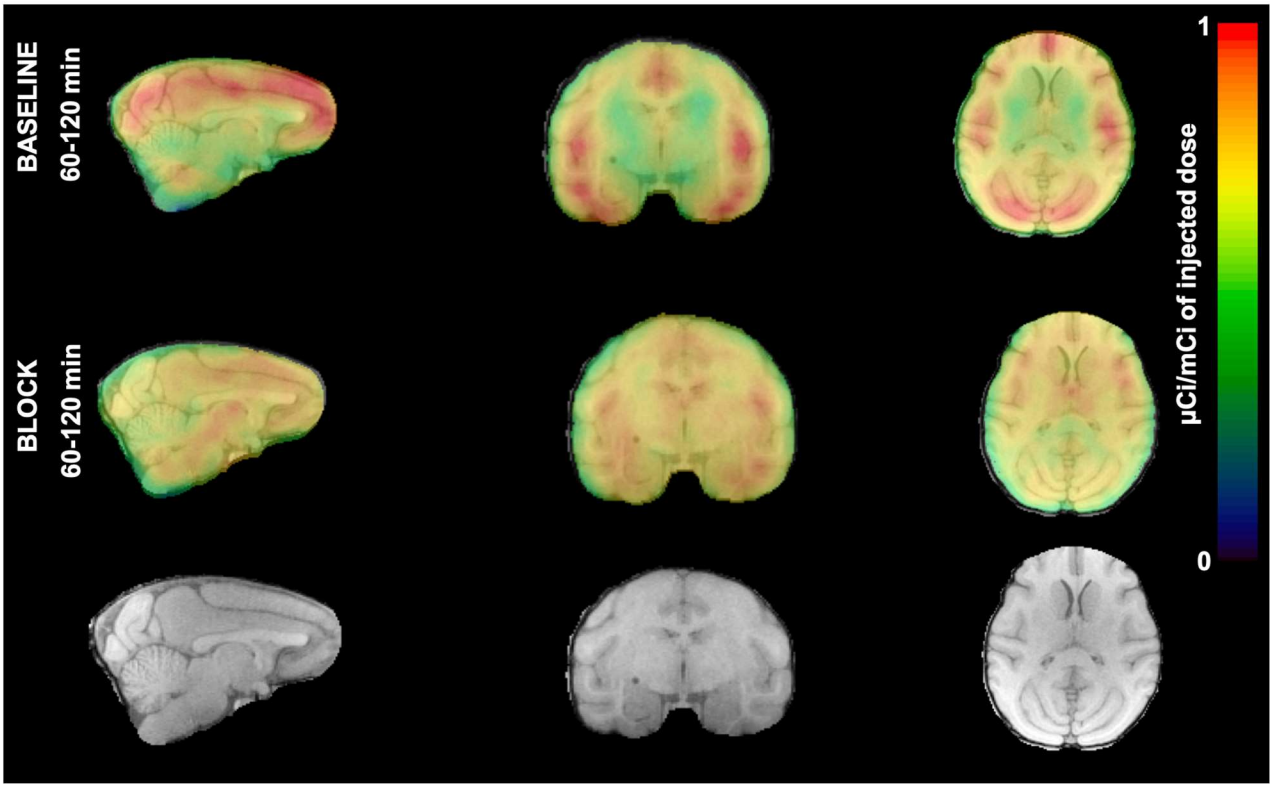

Figure 2. PET and MRI images of [^{11}C]CIMBI-5 in a representative vervet monkey brain; Column 1: Sagittal; Column 2: Coronal; Column 3: Axial; Row 1: Sum of 60-120 minutes PET scan (with overlapped MRI images); Row 2: Sum of 60-120 minutes PET scan after the administration of MDL100907 (with overlapped MRI images); Row 3: MRI images.

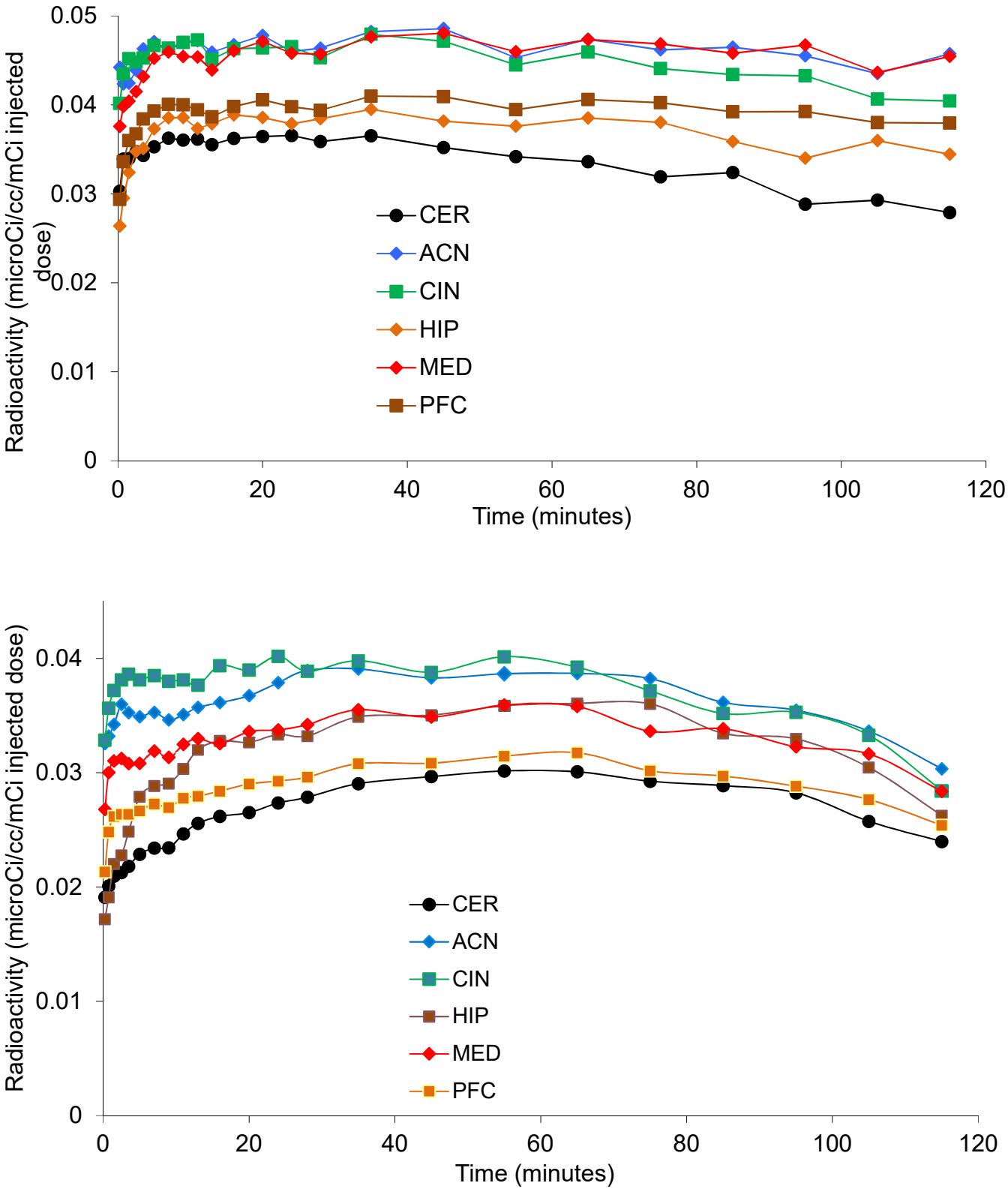

Figure 3. TACs of [^{11}C]CIMBI-5 in a representative vervet monkey at baseline (top) and after blocking with MDL100907 (bottom). (ACN: anterior cingulate; CER: cerebellum; CIN: cingulate cortex; HIP: hippocampus; MED: medial prefrontal cortex; PFC: prefrontal cortex).

Estimates of BP_{NDs} for [^{11}C]CIMBI-5 computed with reference tissue approaches are reported in Figure 4. Logan plot and LEGA methods show comparable results in baseline (n=2) and blocking experiments (n=2) compared with SRTM (Figure 4 A, B and C). A high correlation of BP_{ND} was obtained for [^{11}C]CIMBI-5 baseline and MDL100907 blocking studies between Logan plot and LEGA methods (Figure 4 D). High variations of BP_{ND} were found with the SRTM method (Figure 3D). BP_{NDs} obtained for blocking studies for cortical regions such as DOR, OCC, ORB, PFC, PAR and hippocampus were not in agreement with the distribution of radiotracer based on TAC method.

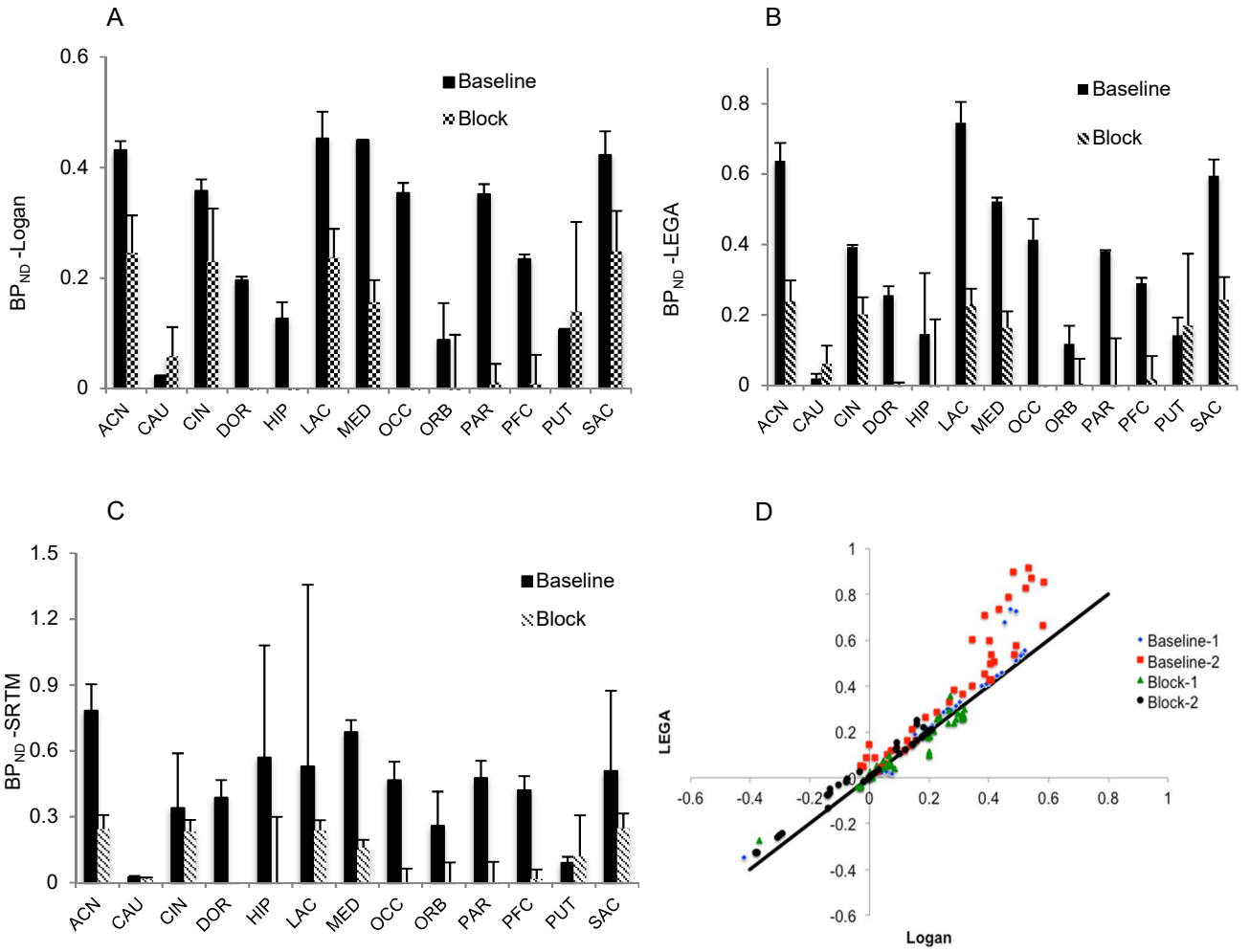

Figure 4. Estimates of [^{11}C]CIMBI-5 BP_{ND} in vervet monkey brain obtained with Logan plot with reference region (A); LEGA with reference region (B); SRTM (C); D: BP_{nd} correlations of Logan plot and LEGA. (ACN: anterior cingulate; CIN: cingulate; DOR: dorsal and lateral prefrontal cortex; HIP: hippocampus; LAC: inferior anterior cingulate; MED: medial prefrontal cortex; OCC: occipital cortex; ORB: orbital cortex; PAR: parietal cortex; PFC: prefrontal cortex; SCA: superior anterior cingulate)

PET studies of [^{11}C]CIMBI-5 in baboon

PET imaging experiments in baboons confirm that [^{11}C]CIMBI-5 penetrates the BBB and accumulates in brain (Figure 5). TACs show that the radiotracer is preferentially retained in 5-HT_{2A}R rich brain regions (Figure 6). Cortical regions show the highest radioligand binding, whereas putamen and cerebellum show the lowest binding. The radioactivity level peaked around 40 min post injection, and target to cerebellar radioactivity ratios at 120 minutes were ~1.5 for most cortical regions (Figure 6). Insular and occipital cortex showed radioactivity ratios of 1.85 and 1.65 with respect to cerebellum at 120 minutes. Slow washout of [^{11}C]CIMBI-5 was observed in cortical regions, where higher density of 5-HT_{2A}R is present.

Relatively faster washout was observed in cerebellum, caudate and putamen, which are regions with comparatively low density of 5-HT_{2A}R. The free fraction of radioligand in plasma was 1-2% (N=2) as determined using the ultracentrifuge method. Fast metabolism and polar metabolites were observed for [^{11}C]CIMBI-5 in baboon plasma. Percentages of unmetabolized parent radioligand were 81% at 2 min, 45% at 12 min, 20% at 30 min, 9% at 60 min and 3% at 90 minute post injection, respectively (Figure 7). The free fraction and percentage of unmetabolized [^{11}C]CIMBI-5 in baboon plasma determined here are in agreement with the values reported for pigs [24,25].

Subsequently, we compared the binding parameters of [^{11}C]CIMBI-5 and [^{11}C]MDL100907 in baboon brain (Figure 8) and the results indicate that V_T, BP_P, and BP_{ND} of [^{11}C]MDL100907 are higher than that of [^{11}C]CIMBI-5, presumably because the antagonist ligand [^{11}C]MDL100907 binds to both high and low

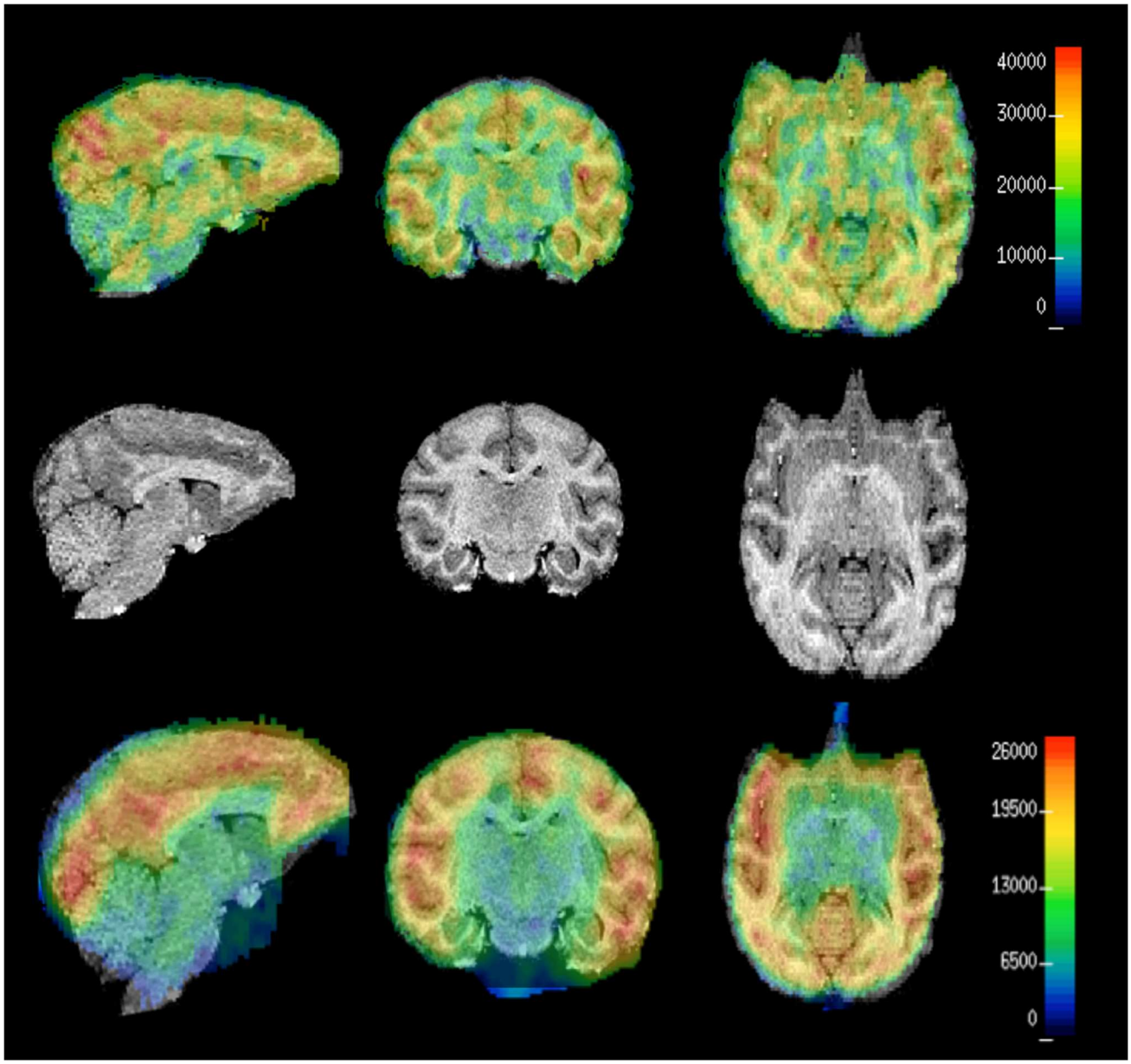

Figure 5. PET images of [^{11}C]CIMBI-5 and [^{11}C]MDL100907 in baboon brain. Top row: Summed [^{11}C]CIMBI-5 PET images of 60-120 minutes (with overlapped MRI images); Middle row: MRI images; Bottom row: Summed [^{11}C]MDL100907 PET images of 60-120 minutes (with overlapped MRI images); Left column: Sagittal, Middle column: Coronal, Right column: Transversal.

affinity states of 5-HT_{2A}R, whereas [^{11}C]CIMBI-5 binds predominantly to the high agonist affinity state of the receptor (Figure 8). A markedly lower BP_P (25%) and BP_{ND} (33%) were observed for [^{11}C]CIMBI-5 scans in comparison with the corresponding [^{11}C]MDL100907 data for 5-HT_{2A}R rich regions in baboon brain. Highest changes of BP_{ND} were found for prefrontal cortex (56.1%), parahippocampal gyrus (PIP) (59.7%) and parietal cortex (61.7%) with corresponding BP_P differences of 66.6%, 69.3% and 70.8% respectively. Caudate, putamen and thalamus showed low BP_P or BP_{ND} with [^{11}C]CIMBI-5 binding vs [^{11}C]MDL100907 binding, may due to low HA 5-HT_{2A}R population in these regions (Figure 8).

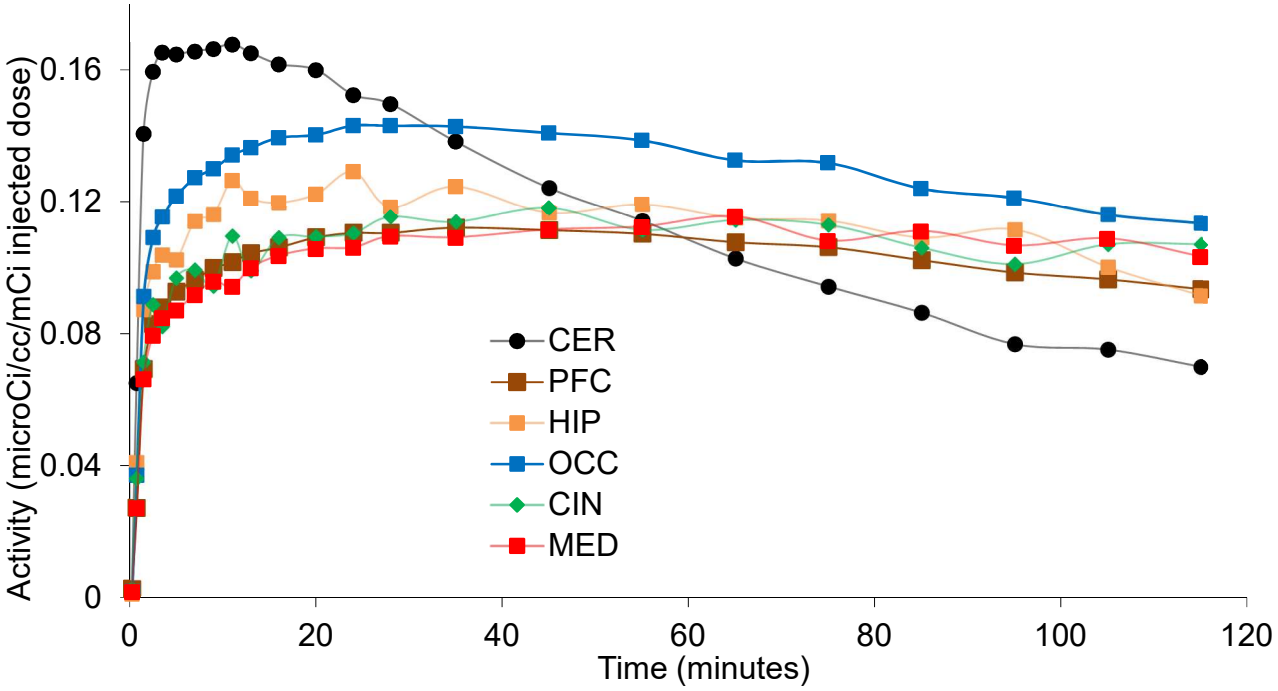

Figure 6. TACs of [^{11}C]CIMBI-5 in baboon brain. (CIN: cingulate; CER: cerebellum; HIP: hippocampus; MED: medial prefrontal cortex; OCC: occipital cortex; PFC: prefrontal cortex)

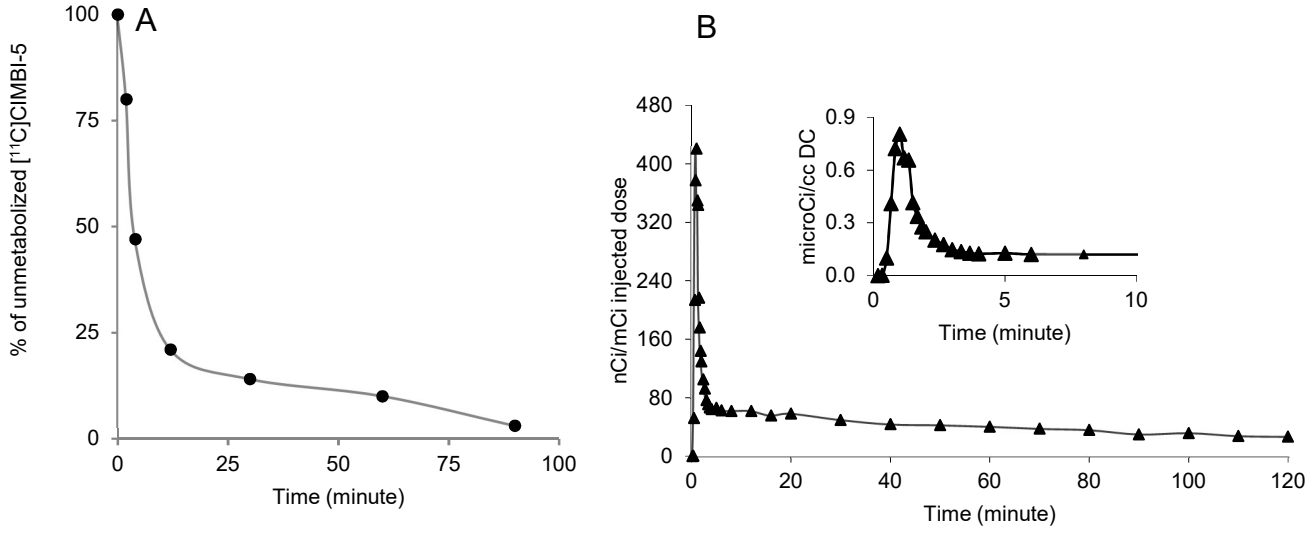

Figure 7. A. Unmetabolized parent fraction of [^{11}C]CIMBI-5 in baboon plasma; B: Metabolite-corrected plasma input curve of [^{11}C]CIMBI-5 in baboon.

DISCUSSION

Here we report the evaluation of [^{11}C]CIMBI-5, the first 5-HT$_{2A}$R agonist PET ligand, in ververt monkey, as well as the comparison of its binding potential to that of the 5-HT$_{2A}$R antagonist PET ligand [^{11}C]M100907 in baboons. The highest and lowest uptake of [^{11}C]CIMBI-5 was observed in cortical regions and in the cerebellum, respectively (Figure 2). The pattern of [^{11}C]CIMBI-5 retention in monkey brain matches the expected distribution of 5-HT$_{2A}$R in brain as well as the distribution reported for the same ligand in pig brain (25). However, washout of the radiotracer in monkey brain was slower than that reported in pig. Although the blocking agents used are different, [^{11}C]CIMBI-5 exhibits similar blockade effect in monkey and pig brain, with the highest specificity in cortex and the lowest in cerebellum and striatum (25). Metabolite analyses of [^{11}C]CIMBI-5 in pig and baboon indicate less lipophilic (polar than the parent CIMBI-5) metabolite. However, *ex vivo* brain homogenate assays in pigs reveal the absence of radioactive metabolite entering the brain, indicating that the sole brain radioactivity in brain is due to parent radioligand. Both Logan plot and LEGA methods show high test retest and test-block reliability for CIMBI-5 in brain in comparison to SRTM. It appears that there is only partial blockade of the 5-HT$_2$ARs with M100907 (Figure 2) and the rate of radiotracer washout from the brain was not significantly affected by the blocking agent even though the absolute uptake was lower (Figure 3). The washout of the radiotracer from the assumed reference region (cerebellum) is also very slow in monkey scans, suggesting the potential presence of off target binding of the radiotracer in the brain. Since 5-HT$_{2B}$Rs are less abundant in brain, the most likely off target for CIMBI-5 is 5-HT$_{2C}$R (Ki= 7 nM) (24).

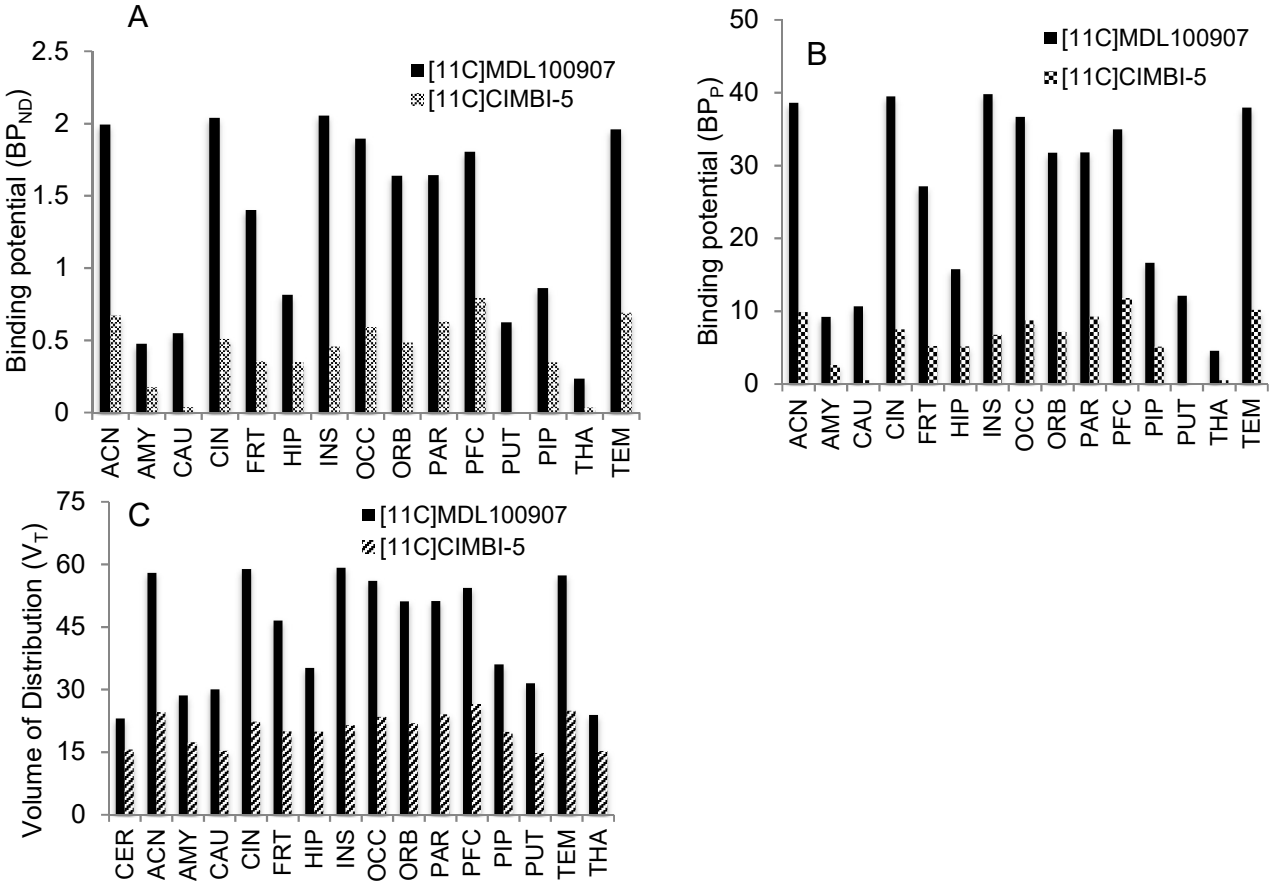

Figures 8: Comparison of estimated values of V_T (C), BP_P (B) and BP_{ND} (A) of [^{11}C]CIMBI-5 and [^{11}C]MDL100907 in baboon (ACN: anterior cingulate; AMY: amygdala; CIN: cingulate; CAU: caudate; CER: cerebellum; FRT: frontal cortex; HIP: hippocampus; INS: insular cortex; OCC: occipital cortex; ORB: orbital cortex; PAR: parietal cortex; PFC: prefrontal cortex; PUT: putamen, PIP: parahippocampal gyrus; THA: thalamus; TEM: temporal cortex.)

The observed distribution of [^{11}C]CIMBI-5 in baboon brain is in agreement with that in vervet monkey and in danish landrace pigs [24,25]. The washout out of the radiotracer in baboon is similar to the one in pig and is faster than the one in monkey (24,25). This is probably due to the different metabolic stability of radiotracer across species. The lower binding potential of [^{11}C]CIMBI-5 in comparison to the antagonist radioligand [^{11}C]MDL100907 is consistent with the high affinity site binding ratio of [^{125}I]DOI (a known 5-HT$_2$R agonist) with [^{3}H]ketanserin and [^{3}H]MDL100907 (antagonists) measured by *in vitro* autoradiography and *in vitro* saturation binding studies (10, 20, 46-49). The lower binding potential of [^{11}C]CIMBI vs. [^{11}C]MDL100907 was similar to that reported for the bromo-analogue [^{11}C]CIMBI-36 and antagonist ligand [^{18}F]altanserin (34). Our studies suggest that [^{11}C]CIMBI-5 binding in brain is comparable to that of [^{11}C]CIMBI-36, and therefore [^{11}C]CIMBI-5 can be useful for occupancy measurement of 5-HT$_{2A}$R. However, both ligands exhibit slow kinetics, limited blocking effect and presence of brain penetrating radiometabolites. Different tracers have different characteristics, such as f_P, free fraction of radioligand in the non-displaceable compartment (f_{ND}), K_D, completion with endogenous 5-HT, brain uptake and washout, interactions with specific or non-specific sites, and so on. Therefore, the observed difference in BP_P and BP_{ND} values of [^{11}C]CIMBI-5 and [^{11}C]MDL100907 could in part arise from the above differences. Although the results reported here show, as a proof of concept, that *in vivo* high affinity agonist site can be imaged using [^{11}C]CIMBI-5 and [^{11}C]CIMBI-36, the development of 5-HT$_{2A}$R agonist PET tracers with improved binding characteristics remains an important goal.

CONCLUSION

We have shown lower binding of 5-HT$_{2A}$R agonist tracer compared to 5-HT$_{2A}$ antagonist tracer in nonhuman primates as measured *in vivo* by PET. We observed target specific distribution of [^{11}C]CIMBI-5 to 5-HT$_{2A}$R in vervet monkey and baboon brains, consistent with the known distribution of 5-HT$_{2A}$R by autoradiography. In general, a markedly lower binding potential is observed for the agonist [^{11}C]CIMBI-5 in comparison with the antagonist [^{11}C]MDL100907 in 5-HT$_{2A}$R rich regions in baboons. The PET imaging data reported here indicate that [^{11}C]CIMBI-5 behaves as a high affinity 5-HT$_{2A}$R agonist tracer in baboon and monkey. The lower binding of the agonist [^{11}C]CIMBI-5 binding in baboon compared to the antagonist [^{11}C]M100907 in this study is consistent with the reported ratio of high affinity site binding of agonists and antagonists by *in vitro* studies, but could also be ascribed to the difference in the free fractions, endogenous completion with 5-HT, and *in vivo* K_D of the radiotracers. Studies comparing *in vivo* B_{max} via Scatchard analyses or endogenous changes of 5-HT$_{2A}$R after pharmacological stimulation would provide further validation of the percentage of HA binding of [^{11}C]CIMBI-5.

CONFLICT OF INTERESTS

None to be declared

ACKNOWLEDGEMENT

The authors would like to thank members of the PET center, Wake Forest School of Medicine, for the monkey PET experiments. This work was funded by NIH grants MH091470, DA041670, P40-OD010965 and UL1-TR001420.

REFERENCES

1. Hoyer D, Hannon JP, Martin GR. Molecular, pharmacological and functional diversity of 5-HT receptors. Pharmacol iochem Behav 2002; 71: 533-554.
2. Nicholas DE. Hallucinogens. Pharmacol Ther 2004; 101: 131-181
3. Meltze HY, Matsubara S, Lee JC. Classification of typical and atypical antipsychotic drugs on the basis of dopamine D-1, D-2 and serotonin2 PKi values. J Pharmacol Exp Ther 1989; 251: 238-246.
4. Bogenschutz MP, Forcehimes AA., Pommy JA, Wilcox CE, Barbosa PCR, Strassman RJ. Psilocybin-assisted treatment for alcohol dependence: a proof-of-concept study. J Psychopharmacol 2015; 29: 289-299.
5. Johnson MW, Garcia-Romeu A, Cosimano MP, Griffiths RR. Pilot study of the 5-HT$_{2A}$R agonist psilocybin in the treatment of tobacco addiction. J Psychopharmacol 2014: 1-10.
6. Bogenschutz MP, Pommy JM. Therapeutic mechanisms of classic hallucinogens in the treatment of addictions: From indirect evidence to testable hypotheses Drug Test Anal 2012: 4; 543–555.
7. Bowen WT, Soskin RA, Chotlos JW. Lysergic acid diethylamide as a variable in the hospital treatment of alcoholism: A follow-up study J Nerv Ment Dis 1970:

150: 111–118.
8. Krebs TS, Johansen P. Lysergic acid diethylamide (LSD) for alcoholism: Meta-analysis of randomized controlled trials J Psychopharm, 2012, 26: 994–1002.
9. Lopez-Gimenez JF, Mengod G, Palacios JM, Vilaro MT. Selective visualization of rat brain 5-HT2A receptors by autoradiography with [3H]MDL 100,907. Naunyn- Schmiedeberg's Arch Pharmacol.1997: 356; 446-454.
10. Roth BL. (Ed) Serotonin receptors: from molecular pharmacology to human therapeutics, Humana press, Totowa, NJ
11. Forutan F, Estalji S, Beu M, Nikolaus S, Hamacher K, Coenen HH, Vosberg H, Müller-Gärtner H-W, Larisch R. Distribution of 5HT2A receptors in the human brain: comparison of data in vivo and post mortem Nuklearmedizin 2002: 41;197–201.
12. Burnet PW, Eastwood SL, Lacey K, Harrison PJ. The distribution of 5-HT1A and 5-HT2A receptor mRNA in human brain Brain Res 1995: 676; 157-1168.
13. Gonzalez-Maeso J, Weisstaub NV, Zhou M, Chan P, Iviv L, Ang R, Lira A, Bradley-Moore M, Ge Y, Zhou Q, Sealfon SC, Gingrich JA. Hallucinogens recruit specific cortical 5-HT(2A) receptor-mediated signaling pathways to affect behavior Neuron 2007:53;439–452.
14. Abbas A, Roth BL. Pimavanserin tartrate: a 5-HT2A inverse agonist with potential for treating various neuropsychiatric disorders Expert Opin Pharmacother 2008: 9; 3251–9.
15. Jones BJ, Blackburn TP. The medical benefit of 5-HT research. Pharmacol Biochem Behav 2002: 71; 555-568.
16. Leysen JE. Curr Drug Targets CNS Neurol Disord 2004: 3; 11-26.
17. Paterson LM, Kornum BR, Nutt DJ, Pike VW, Knudsen GM. 5-HT Radioligands for Human Brain Imaging With PET and SPECT *Med Res Rev* 2013: 33(1); 54-111.
18. Kumar JSD, Mann JJ. PET Tracers for Serotonin Receptors and Their Applications Cent Nerv Sys Agents Med Chem 2014: 14(2); 96-112.
19. Herth MH, Knudsen GM. Current radiosynthesis strategies for 5-HT_{2A} receptor PET tracers J Label Comp Radiopham 2015: 58(7); 265-273.
20. Lopez-Gimenez JF, Villazon M, Brea J, Loza MI, Palacios JM, Mengold G, Vilaro M. Multiple conformations of native and recombinant human 5-hydroxytryptamine (2a) receptors are labeled by agonists and discriminated by antagonists Mol Pharmacol 2001: 60; 690–699.
21. Laruelle M. Imaging synaptic neurotransmission with in vivo binding competition techniques: a critical review J Cereb Blood Flow Metab 2000: 20; 423-451.
22. Paterson LM, Tyacke RJ, Nutt DJ, Knudsen GM. Measuring endogenous 5-HT release by emission tomography: promises and pitfalls J Cereb Blood Flow Metab 2010: 30(10); 1682-1706.
23. Barnes NM, Sharp T. A review of central 5-HT receptors and their function Neuropharmacol 1997: 18; 583-587.
24. Ettrup A, Hansen M, Santini MA, Paine J, Gillings N, Palner M, Lehel S, Herth MM, Madsen J, Kristensen J, Begtrup M, Knudsen GM. Radiosynthesis and in vivo evaluation of a series of substituted 11C-phenethylamines as 5-HT (2A) agonist PET tracers Eur J Nucl Med Mol Imaging 2011: 38 (4); 681–693.
25. Ettrup A, Palner M, Gillings N, Santini MA, Hansen M, Kornum BR, Rasmussen LK, Nagren K, Madsen J, Begtrup M, Knusdsen GM. Radiosynthesis and evaluation of 11C-CIMBI-5 as a 5-HT2A receptor agonist radioligand for PET J Nucl Med 2010: 51(11);1763-70.
26. Prabhakaran J, Majo VJ, Milak MM, Gillings N, Ettrup A, Prem S, Mann JJ, Parsey RV, Knudsen GM, Kumar JSD. Radiosynthesis and evaluation of [11C]CIMBI-5 as a 5-HT2A agonist PET tracer. J Nuc Med 2012: 53; (supplement 1), 1876.
27. Prabhakaran J, Majo VJ, Milak MM, Gillings N, Ettrup A, Mann JJ, Parsey RV, Knudsen GM, Kumar JSD. Quantification [11C]CIMBI-5, a 5-HT2AR agonist PET ligand in vervet monkey 2015: 56 (supplement 3), 1558.
28. Ettrup A, Holm S, Hansen M, Wasim M, Santini MA, Palner M, Madsen J, Svarer C, Kristensen JL, Knudsen GM. Preclinical safety assessment of the 5-HT2A receptor agonist PET radioligand [(11)C]Cimbi-36 *Mol Imaging Biol* 2013: 15 (4); 376–383.
29. Finnema SJ, Stepanov V, Ettrup A, Nakao R, Amini N, Svedber M, Lehman C, Hansen M, Knudsen GM, Halldin C. Characterization of [C-11]CIMBI36 as an agonist PET radioligand for the 5-HT2A and 5-HT2C receptors in the nonhuman primate brain Neuroimage 2014: 84, 342-353.
30. Jorgensen LM, Weikop P, Villadsen J, Visnapuu T, Ettrup A, Hansen HD, Baandrup AO, Andersen FL, Bjarkam CR, Thomsen C, Jespersen B, Knudsen GM. Cerebral 5-HT release correlates with [11C]Cimbi36 PET measures of 5-HT2A receptor occupancy in the pig brain. J Cereb Blood Flow Metab. 2017;37(2):425-434.
31. Yang KC, Stepanov V, Martinsson S, Ettrup A, Takano A, Knudsen GM, Halldin C, Farde L, Finnema SJ. Fenfluramine Reduces [11C]Cimbi-36 Binding to the 5-HT2A Receptor in the Nonhuman Primate Brain. Int J Neuropsychopharmacol. 2017;20(9):683-691.
32. Ettrup A, Bang S-C, McMahon B, Lehel S, Dyssegaard A, Skibsted AW, Jørgensen L M, Hansen M, Baandrup AO, Bache S, Svarer C, Kristensen JL, Gillings N, Madsen J, Knudsen GM. Serotonin 2A receptor agonist binding in the human brain with [11C]Cimbi-36 J Cer Blood Flow Metab 2014: 34;

1188–1196.
33. Ettrup A, Svarer C, McMahon B, da Cunha-Bang S, Lehel S, Muller K, Dyssegaard A, Ganz M, Beliveau V, Jorgensen LM, Gillings N, Knudsen GM. Serotonin 2A receptor agonist binding in the human brain with [(11)C]Cimbi-36: Test-retest reproducibility and head-to-head comparison with the antagonist [(18)F]altanserin. Neuroimage. 2016;130:167-174.
34. Prabhakaran J, Underwood MD, Kumar JSD, Simpson NR, Kassir SA, Bakalian MJ, Mann JJ, Arango V. Synthesis and in vitro evaluation of [18F] FECIMBI-36: A potential agonist PET ligand for 5-HT2A/2C receptors, Bioorg Med Chem Let 2015: 25(18); 3933-3936.
35. Petersen IN, Villadsen J, Hansen HD, Jensen AA, Lehel S, Gillings N, Herth MM, Knudsen GM, Kristensen JL. Convergent 18F-labeling and evaluation of N-benzyl-phenethylamines as 5-HT2Areceptor PET ligands. Bioorg Med Chem. 2016;24(21):5353-5356.
36. Herth MM, Petersen IN, Hansen HD. Hansen M, Ettrup A, Jensen AA, Lehel S, Dyssegaard A, Gillings N, Knudsen GM, Kristensen JL. Synthesis and evaluation of (18)F-labeled 5-HT2A receptor agonists as PET ligands. Nucl Med Biol. 2016, 43(8):455-62.
37. Prabhakaran J, Solingapuram Sai KK, Zanderigo F, Rubin-Falcone H, Jorgensen MJ, Kaplan JR, Tooke KI, Mintz A, Mann JJ, Kumar JSD. In vivo evaluation of [18F]FECIMBI-36, an agonist 5-HT2A/2C receptor PET radioligand in nonhuman primate. Bioorg Med Chem Lett. 2017;27(1):21-23.
38. Gandelman MS, Baldwin RM, Zoghbi SS, Zea-Ponce Y, Innis RB. Evaluation of ultrafiltration for the free-fraction determination of single photon emission computed tomography (SPECT) radiotracers beta-CIT, IBF, and iomazenil. J Pharm Sci 1994; 83: 1014–1019.
39. Watabe H, Channing MA, Der MG, Adams HR, Jagoda E, Herscovitch P, Eckelman WC, Carson RE. Kinetic analyses of the 5-HT2A ligand [11C]MDL 100907. J Cereb Blood Flow Metab 2000; 20(6): 899-909.
40. Watson CC, Newport D, Casey ME. A single scatter simulation technique for scatter correction in 3D PET. In: Grangeat P, Amans J-L, (Eds.). Fully three-dimensional image reconstruction in radiology and nuclear medicine. Dordrecht Kluwer Academic 1995; 215– 9.
41. Mawlawi O, Martinez D, Slifstein M, Broft A, Chatterjee R, Hwang DR, Huang Y, Simpson NR, Ngo K, Van Heertum RL, Laruelle M. Imaging human mesolimbic dopamine transmission with positron emission tomography: I. Accuracy and precision of D(2) receptor parameter measurements in ventral striatum. J Cereb Blood Flow Metab 2001; 21; 1034– 57.
42. Woods RP, Cherry SR, Mazziotta JC. Rapid automated algorithm for aligning and reslicing PET images J Comput Assist Tomor 1992; 16: 20-33.
43. Ogden RT. On estimation of kinetic parameters in graphical analysis of PET imaging data. Stat Med 2003; 22: 3557–3568.
44. Parsey RV, Ogden RT, Mann JJ. Determination of volume of distribution using likelihood estimation in graphical analysis: elimination of estimation bias. J Cereb Blood Flow Metab 2003; 23: 1471–1478.
45. Mintun MA, Raichle ME, Kilbourn MR, Wooten GF, Welch MJ. A quantitative model for the in vivo assessment of drug binding sites with positron emission tomography. Ann Neurol 1984; 15: 217-227.
46. Appel NM, Mitchell WM, Garlick RK, Glennon RA, Teitler M, De Souza EB. Autoradiographic characterization of (+-)-1-(2,5-dimethoxy-4-[125I] iodophenyl)-2-aminopropane ([125I]DOI) binding to 5-HT2 and 5-HT1c receptors in rat brain. J Pharmacol Exp Ther 1990; 255(2): 843-57.
47. Shi J, Damjanoska KJ, Singh RK, Carrasco GA, Garcia F, Grippo AJ, Landry M, Sullivan NR., Battaglia G., Muma NA. Agonist induced-phosphorylation of G□11 protein reduces coupling to 5-HT2A rceptors. J Pharmacol and Exp Therap 2007; 323(1): 248-256.
48. Lopez-Gimenez JF, Vilaro MT, Palacios JM, Mengod G. Multiple conformations of 5-HT2A and 5-HT2C receptors in rat brain: an autoradiographic study with [125I](±)DOI. Exp Brain Res 2013; 230(4): 395-406.
49. McKenna DJ, Peroutka SJ. Differentiation of 5-Hydroxytryptamine, Receptor Subtypes Using125l-R-(-)2,5-Dimethoxy-4-iodo-phenylisopropylamine and 3H-Ketanserin. J Nueurosci 1999; 9(10): 3482-3490.
50. Innis RB, Cunningham VJ, Delforge J, Fujita M, Gjedde A, Gunn RN, Holden J, Houle S, Huang SC, Ichise M, Iida H, Ito H, Kimura Y, Koeppe RA, Knudsen GM, Knuuti J, Lammertsma AA, Laruelle M, Logan J, Maguire RP, Mintun MA, Morris ED, Parsey R, Price JC, Slifstein M, Sossi V, Suhara T, Votaw JR, Wong DF, Carson RE. Consensus nomenclature for in vivo imaging of reversibly binding radioligands. J Cereb Blood Flow Metab. 2007;27(9):1533-1539.